



## **The leucine-rich repeat domain of human peroxidase 1 promotes binding to laminin in basement membranes**

Sevcnikar, Benjamin; Schaffner, Irene; Chuang, Christine Y.; Gamon, Luke; Paumann-Page, Martina; Hofbauer, Stefan; Davies, Michael J.; Furtmüller, Paul G.; Obinger, Christian

*Published in:*

Archives of Biochemistry and Biophysics

*DOI:*

[10.1016/j.abb.2020.108443](https://doi.org/10.1016/j.abb.2020.108443)

*Publication date:*

2020

*Document version*

Publisher's PDF, also known as Version of record

*Document license:*

[CC BY-NC-ND](https://creativecommons.org/licenses/by-nc-nd/4.0/)

*Citation for published version (APA):*

Sevcnikar, B., Schaffner, I., Chuang, C. Y., Gamon, L., Paumann-Page, M., Hofbauer, S., ... Obinger, C. (2020). The leucine-rich repeat domain of human peroxidase 1 promotes binding to laminin in basement membranes. *Archives of Biochemistry and Biophysics*, 689, [108443]. <https://doi.org/10.1016/j.abb.2020.108443>



# The leucine-rich repeat domain of human peroxidasin 1 promotes binding to laminin in basement membranes

Benjamin Sevcnikar<sup>a</sup>, Irene Schaffner<sup>a</sup>, Christine Y. Chuang<sup>b</sup>, Luke Gamon<sup>b</sup>,  
Martina Paumann-Page<sup>c</sup>, Stefan Hofbauer<sup>a</sup>, Michael J. Davies<sup>b</sup>, Paul G. Furtmüller<sup>a,\*\*</sup>,  
Christian Obinger<sup>a,\*</sup>

<sup>a</sup> Department of Chemistry, Institute of Biochemistry, BOKU – University of Natural Resources and Life Sciences, Muthgasse 18, A-1190, Vienna, Austria

<sup>b</sup> Department of Biomedical Sciences, University of Copenhagen, Copenhagen, Denmark

<sup>c</sup> Department of Pathology and Biomedical Science, University of Otago, Christchurch, New Zealand

## ARTICLE INFO

### Keywords:

Human peroxidasin 1  
Extracellular matrix  
Basement membrane  
Type-IV collagen  
Laminin  
Immunoprecipitation  
Surface plasmon resonance spectroscopy

## ABSTRACT

Human peroxidasin 1 (PXDN) is a homotrimeric multidomain heme peroxidase and essential for tissue development and architecture. It has a biosynthetic function and catalyses the hypobromous acid-mediated formation of specific covalent sulfilimine (S=N) bonds, which cross-link type IV collagen chains in basement membranes. Currently, it is unknown whether and which domain(s) [i.e. leucine-rich repeat domain (LRR), immunoglobulin domains, peroxidase domain, von Willebrand factor type C domain] of PXDN interact with the polymeric networks of the extracellular matrix (ECM), and how these interactions integrate and regulate the enzyme's cross-linking activity, without imparting oxidative damage to the ECM. In this study, we probed the interactions of four PXDN constructs with different domain compositions with components of a basement membrane extract by immunoprecipitation. Strong binding of the LRR-containing construct was detected with the major ECM protein laminin. Analysis of these interactions by surface plasmon resonance spectroscopy revealed similar kinetics and affinities of binding of the LRR-containing construct to human and murine laminin-111, with calculated dissociation constants of 1.0 and 1.5  $\mu\text{M}$ , respectively. The findings are discussed with respect to the recently published in-solution structures of the PXDN constructs and the proposed biological role of this peroxidase.

## 1. Introduction

Basement membranes (BMs) are widely-distributed cell-adherent specialized extracellular matrices (ECMs), that provide a complex framework that segregates polarized epithelial or endothelial cells from the underlying mesenchyme [1,2]. The emergence of BMs coincided with the origin of multicellularity in animals, suggesting that they are essential for the formation of tissues. BMs provide structural support to tissues and play active roles in many developmental processes including organogenesis, angiogenesis and tissue repair [3]. Their sheet-like structure derives from two independent polymeric networks derived from two major protein classes: the laminins and type IV collagen [4]. These (independent) networks interact with each other via additional ECM proteins including agrin, nidogen, entactin and perlecan [3].

Laminins are cross-shaped heterotrimers ( $\alpha\beta\gamma$ ) that share a common structure with a number of globular and rod-like domains [5,6]. In vertebrates, five  $\alpha$ , three  $\beta$ , and three  $\gamma$  chains are assembled in

different combinations generating a large variety of isoforms which are believed to have distinct functions in embryogenesis, vascular maturation, and neuromuscular development [7]. For example, the isoform laminin-111 (i.e.  $\alpha1\beta1\gamma1$ ) plays an important role in the early embryonic development in mammals [7].

Previous studies have shown that the ECM proteins are highly susceptible to oxidative damage due to their high abundance, their low rate of turnover, and the relatively low levels of extracellular antioxidants, repair and catabolic systems [8]. Oxidants can induce structural and functional changes to laminins and other ECM materials, with damage evident in multiple tissue samples, including human atherosclerotic lesions [9–11]. It has been hypothesized that co-localisation of hypohalous acid-producing myeloperoxidase (MPO) with ECM components might be involved in the observed oxidative damage, since MPO undergoes transcytosis across endothelial cells and binds tightly to sub-endothelial and glomerular BM [12] and particularly fibronectin [13]. MPO also directly binds to perlecan via an electrostatic

\* Corresponding author.

\*\* Corresponding author.

E-mail addresses: [paul.furtmueller@boku.ac.at](mailto:paul.furtmueller@boku.ac.at) (P.G. Furtmüller), [christian.obinger@boku.ac.at](mailto:christian.obinger@boku.ac.at) (C. Obinger).

<https://doi.org/10.1016/j.abbi.2020.108443>

Received 25 February 2020; Received in revised form 26 May 2020; Accepted 27 May 2020

Available online 30 May 2020

0003-9861/ © 2020 The Authors. Published by Elsevier Inc. This is an open access article under the CC BY-NC-ND license

(<http://creativecommons.org/licenses/by-nc-nd/4.0/>).

**Abbreviations**

PXDN	human peroxidase 1
LRR	leucine-rich repeat domain
Ig	immunoglobulin domain
VWC	C-terminal von Willebrand factor type C
POX	peroxidase domain
ECM	extracellular matrix
BM	basement membrane
BME	basement membrane extract
LN	laminin
huLN	human laminin
muLN	murine laminin

MPO	myeloperoxidase
LPO	lactoperoxidase
EPO	eosinophil peroxidase
TPO	thyroid peroxidase
PBS	phosphate buffer-saline
PBST	phosphate buffer-saline + Tween 20
IP	immunoprecipitation
SAXS	small-angle X-ray scattering
SPR	surface plasmon resonance
SEC-MALS	size exclusion chromatography combined with multi-angle light scattering
MCK	multi-cycle kinetics

interaction established between cationic MPO and the anionic side chains of perlecan [14].

Recently, a related human peroxidase, peroxidase 1 (PXDN) was detected within the ECM network [15,16]. In contrast to MPO (which exhibits antimicrobial activity and is part of the innate immune system), PXDN has been shown to have a biosynthetic function and to mediate the formation of specific covalent sulfilimine (S=N) bonds that cross-link type IV collagen chains in BMs. In contrast to MPO (and other homologous human peroxidases), PXDN is a multi-domain, highly-glycosylated, homotrimeric peroxidase [17,18] and a member of Family 2 of the peroxidase-cyclooxygenase superfamily [19,20]. It catalyses the hydrogen peroxide-mediated oxidation of bromide to hypobromous acid [21], which mediates S=N bond formation between specific (hydroxy)lysine and methionine residues at the interface of two NC1-domain trimers of type IV collagen [15,16,22]. Removal of the substrate bromide, and hence prevention of cross-linking, is embryonically lethal in *Drosophila melanogaster* and *Caenorhabditis elegans* [16]. Thus, peroxidase 1 catalyses a post-translational modification that is essential for tissue development and architecture.





To date, it is unknown how peroxidase 1 is embedded in the ECM, and how it is able to catalyse the formation of specific sulfilimine bonds in type IV collagen without inducing (collateral) oxidative damage to other sites on the collagen chains, or other BM molecules. In particular, the role(s) of specific PXDN-typical domains, including the N-terminal leucine-rich repeat domain (LRR), the immunoglobulin domains (Ig), and the C-terminal von Willebrand factor type C module (VWC) [17,18], which are all known to be important for protein-protein interactions and cell adhesion [22], are unknown. Therefore, we have designed and produced four recombinant and truncated PXDN variants with different domain compositions in order to identify potential BM binding partners by co-immunoprecipitation (IP). We have unambiguously identified laminin as a binding partner of PXDN and demonstrate that the LRR domain promotes high affinity binding to murine and human laminin-111 with very similar  $K_D$  values, as determined by surface plasmon resonance (SPR) spectroscopy.

**2. Material and methods****2.1. Materials**

High purity murine laminin (muLN111) free of entactin (Corning® Ultrapure Laminin) was purchased from Corning Incorporated, USA. Human laminin isoforms (huLN111, huLN411) were from Biolamina AB, Sweden. Laminin concentrations were determined via the UV-vis absorption at 280 nm and based on molar masses of 900 and 713 kDa (muLN111 and huLN111) or 579 kDa (huLN411). Murine basement membrane extract (BME) with reduced growth factors (Cultrex) was purchased from Trevigen. Protein G Dynabeads were obtained from ThermoFisher. The anti-His<sub>6</sub> antibody monoclonal antibody and rabbit anti-laminin polyclonal antibody, were purchased from Abcam, and the secondary anti-rabbit IgG conjugated with horseradish peroxidase antibody was purchased from GE. Other chemicals were purchased from Sigma at the highest grade available.

**2.2. Cloning, expression and purification of constructs**

We have cloned and recombinantly produced four PXDN constructs, namely PXDN-con2, PXDN-con3, PXDN-con4, and PXDN-con5 (Fig. 1). UniProt KB (<http://www.uniprot.org/>) data on human peroxidase 1 (Q92626) provided the basis for primer design. DNA of PXDN-con 2 (Pro<sup>246</sup>-Leu<sup>1471</sup>), PXDN-con 3 (Val<sup>27</sup>-Asp<sup>1314</sup>), PXDN-con 4 (Pro<sup>246</sup>-Asp<sup>1314</sup>) and PXDN-con 5 (Gly<sup>619</sup>-Asp<sup>1314</sup>) were cloned into a modified gWiz vector (Genlantis) carrying an N-terminal His<sub>6</sub> tag for protein purification. Forward and reverse PCR primers were as follows: PXDN-con2: 5'-gaggctcaccac-caccatcac catccccgaatcacctccgagccc -3' and 5'-agccagaagtgatctgactca-taagcagactggacagcaggc-3'; PXDN-con3: 5'-gaggctcaccaccaccatcaccatgtgg-tggcccagaagccggg-3' and 5'-tagccagaagtgatctgactcagctctgccaccgccggagtc-3'; PXDN-con4: 5'-gctctgggtccagggtccactggccatcaccatcaccatggagatcc-gttgtagctacctcatcg-3' and 5'-gccagaggtcaggtcggggatccttatcagctctcca-caccggaggtccaccctgggg-3'; PXDN-con5: same forward primer as for PXDN-con5 and 5'-gccagaggtcaggtcggggatccttaactgag-cggtgattcaagttctttatc-3'. Transformed *E. coli* XL-10 were screened via colony-PCR and positive clones were selected and validated by DNA sequencing.

Construct	Domain composition of the constructs	MW (kDa)	Oligomeric structure
PXDN -con2		138	Trimer
PXDN -con3		145	Monomer
PXDN -con4		120	Monomer
PXDN -con5		81	Monomer

**Fig. 1. Overview of the investigated constructs of human peroxidase-1.** PXDN-con2 comprises four immunoglobulin (Ig) domains and the peroxidase domain (POX) as well as the C-terminal von Willebrand factor type C (VWC) domain and forms trimers; PXDN-con3 is monomeric and comprises the leucine rich repeat domain (LRR), the Ig domains and POX; PXDN-con4 is monomeric and consists of the four Ig domains and POX; PXDN-con5 is monomeric and consists of the catalytic peroxidase domain only.

For recombinant expression, we chose the HEK 293F (Invitrogen) suspension system. Cells were cultivated according to the Invitrogen User Guideline. Cells were transfected as reported previously [21]. Hemin chloride was added to the culture medium to a final concentration of  $5 \mu\text{g mL}^{-1}$  4 h after transfection to improve heme incorporation. Supernatants were harvested 5 days after transfection. Purification of the different constructs (Fig. 1) followed a procedure described previously [21,23]. In short, the harvested supernatant was filtrated through a  $0.45 \mu\text{m}$  PVDF membrane (Durapore) and concentrated to 100 mL using a Millipore Labscale TFF diafiltration system. Subsequently, the sample was adjusted to 1 M NaCl and 20 mM imidazole.

For purification of the His<sub>6</sub>-tagged proteins, 5 mL HisTrap FF columns (GE Healthcare) loaded with nickel chloride were used. After equilibration of the column with 100 mM sodium phosphate buffer (pH 7.4) containing 1 M NaCl and 20 mM imidazole, the sample was loaded and washed with equilibration buffer. The protein was eluted using two consecutive step gradients of 8% and 70% of 20 mM sodium phosphate buffer, pH 7.4, 500 mM NaCl and 500 mM imidazole. Eluted fractions were analysed by UV-vis spectroscopy and SDS-PAGE. Appropriate fractions were pooled and washed 5 times with 100 mM sodium phosphate buffer, pH 7.4, using Amicon Ultra-15 50 kDa cut-off centrifugal filters (Merck Milipore).

### 2.3. Immunoprecipitation

Murine basement membrane extract (BME; 20  $\mu\text{g}$ ) was mixed with 10  $\mu\text{g}$  of each construct and incubated at 21 °C for 1 h. Protein G Dynabeads (ThermoFisher) were coupled with an anti-His<sub>6</sub> antibody (Abcam mouse 1  $\times$  Anti-6  $\times$  His tag<sup>®</sup>) according to the manufacturer's protocol and was washed once with 0.05% v/v Tween 20 in PBS (PBST). The BME-construct mix was subsequently added to the coupled Dynabeads and immunoprecipitated overnight with rotation at 4 °C. On the next day, samples were washed 3 times with PBST, transferred into clean tubes and eluted from the Protein G Dynabeads using the elution buffer as per manufacturer's protocol to collect the immunoprecipitate.

### 2.4. Silver staining and immunoblotting

Immunoprecipitated samples were treated with NuPAGE reducing buffer (1:10 dilution; ThermoFisher) and heat denatured for 10 min at 70 °C in the presence of the NuPAGE sample buffer (1:4 dilution; ThermoFisher) and loaded onto NuPAGE 3–8% Tris-acetate gels run under constant voltage (160 V) for 70 min. High molecular mass protein markers (HMW HiMark; 460–31 kDa; ThermoFisher) were used as calibration standards. Protein bands were detected by both silver staining and immunoblotting using a rabbit polyclonal anti-laminin antibody (Abcam ab11575, 1:2000 dilution) and an anti-rabbit-HRP conjugated secondary antibody (1:5000 dilution), with the blots developed using a commercial chemiluminescence (ECL) reagent (PerkinElmer, MA, USA), and imaged using a chemiluminescence imager (Syngene, MD, USA).

### 2.5. Surface plasmon resonance

Surface plasmon resonance (SPR) experiments were performed on a Biacore T200 instrument (GE Healthcare). Laminin variants ( $10 \mu\text{g mL}^{-1}$  in 10 mM sodium acetate buffer, pH 4.5) were covalently immobilized on flow cells 2, 3 and 4 (immobilization levels: muLN111 ~ 2650 RU; huLN111 ~ 2015 RU; huLN411 ~ 1615 RU), on a commercially available CM5 chip (GE Healthcare) using the amine coupling kit according to the manufacturer's protocol (GE Healthcare). In short, the flow cells were activated with 1-ethyl-3-[3-dimethylaminopropyl] carbodiimide (EDC)/N-hydroxysulfosuccinimide (NHS) and excess reactive carboxyl groups were blocked with ethanolamine. Flow cell 1 was activated and blocked in the same way and served as reference surface (without ligand). Multi-cycle kinetics (MCK) experiments were performed at 25 °C using increasing concentrations of PXDN-con3, PXDN-con4, and PXDN-con5 respectively (0.14; 0.281; 0.5625; 1.125; 2.25; 4.5; 9  $\mu\text{M}$ ). 1  $\times$  PBS supplemented with 0.05% Tween 20 was used as running buffer. Double referencing was accomplished by subtracting the signal from injections of running buffer. The flow rate was set to  $30 \mu\text{L min}^{-1}$ , association time was 7 min, dissociation was monitored for 20 min. Complete regeneration of laminin variants was achieved by one injection of glycine-HCl, pH 1.5 (30 s,  $30 \mu\text{L min}^{-1}$ ) followed by four injections of 10 mM NaOH (30 s each,  $30 \mu\text{L min}^{-1}$ )

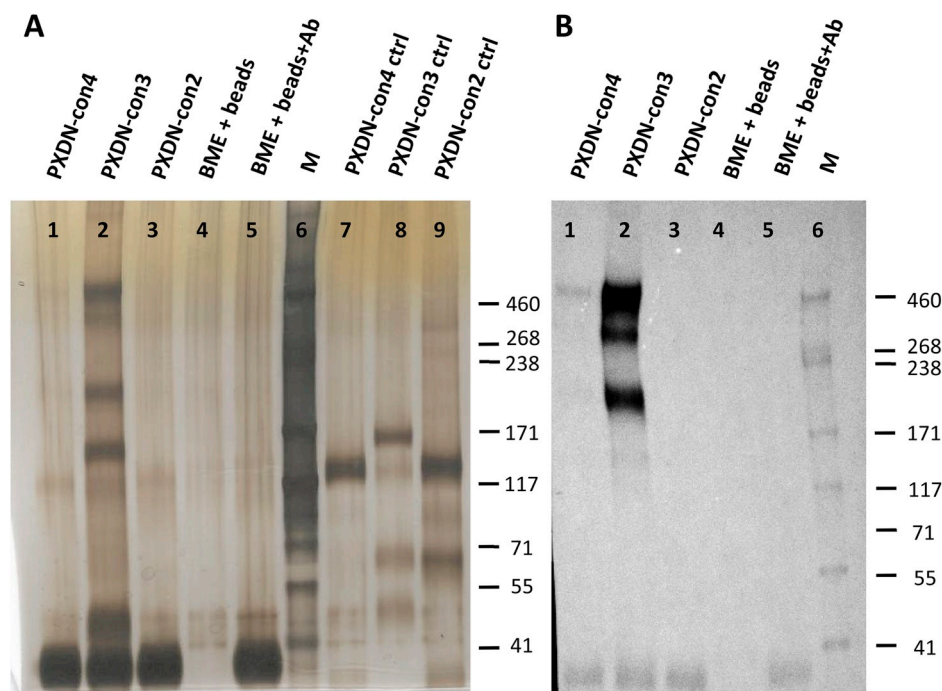


**Fig. 2. Immunoprecipitation of truncated human peroxidasin-1 variants and basement membrane extracts.** (A) Silver-stained SDS-PAGE under reducing conditions. Lanes 1–3 show immunoprecipitates containing monomeric PXDN-con4, monomeric PXDN-con3 or trimeric PXDN-con2. Lanes 4 and 5 represent negative controls. BME, basement membrane extract; Ab, anti-His<sub>6</sub> antibody. Lane 6: marker proteins. Lanes 7–9: SDS-PAGE of recombinant glycosylated constructs only (ctrl, control). (B) Immunoblot using anti-laminin polyclonal antibody. Lanes 1–3 show immunoprecipitates containing monomeric PXDN-con4, monomeric PXDN-con3 or trimeric PXDN-con2. Lanes 4 and 5 represent negative controls and lane 6 marker proteins. All gels and blots are representatives of at least three independent experiments.

after every cycle. The integrity of the various ligands within one titration experiment was ensured by testing reproducibility of the 1.125  $\mu\text{M}$  analyte binding curve after application of the highest analyte concentration. Data were analysed with the Biacore Evaluation Software version 3.1 (GE Healthcare). To determine the dissociation constant  $K_D$ , steady-state response units were plotted against analyte concentrations and the data were fitted to a steady-state affinity model. All MCK experiments were performed in triplicates.

### 3. Results

The truncated constructs PXDN-con2, PXDN-con3, PXDN-con4, and PXDN-con5 (Fig. 1) with an N-terminal His<sub>6</sub> tag were purified using affinity chromatography and preparative size exclusion chromatography (SEC). PXDN-con2 forms trimers, whereas PXDN-con3, PXDN-con4 and PXDN-con5 are monomeric proteins. Importantly, full length homotrimeric PXDN is not included in this study because we (and also other groups) have not been able to obtain sufficient amounts of correctly folded protein. The correct folding of the recombinant proteins were probed routinely by SEC coupled to multi-angle light scattering

(MALS), circular dichroism and UV-vis spectroscopy as described recently [21,23].

#### 3.1. Laminin is a specific binding partner of human peroxidasin 1 (PXDN)

Purified distinct His<sub>6</sub>-tagged PXDN constructs were mixed with murine extracellular basement membrane extract (which contains laminins, collagen IV, entactin and heparan sulphate proteoglycans) and incubated with protein G coated with an anti-His<sub>6</sub> antibody. The mixture was immunoprecipitated, the attached proteins released, and these then separated by electrophoresis under reducing conditions. Fig. 2A compares the silver-stained IP mixtures with positive controls (ctrl) of pure recombinant glycosylated constructs 2, 3 and 4 which have molar masses of 130–170 kDa (right side of panel A). It has been demonstrated that the full length PXDN has ten confirmed N-glycosylation sites [seven on the peroxidase domain (POX), one on the Ig domains, one in the C-terminal linker region between POX and the VWC module and one on the VWC module] [18]. From the IP mixtures, only PXDN-con3 (molar mass of glycosylated protein  $\sim$ 170 kDa) showed three additional bands at molar masses  $\gg$  170 kDa suggesting co-

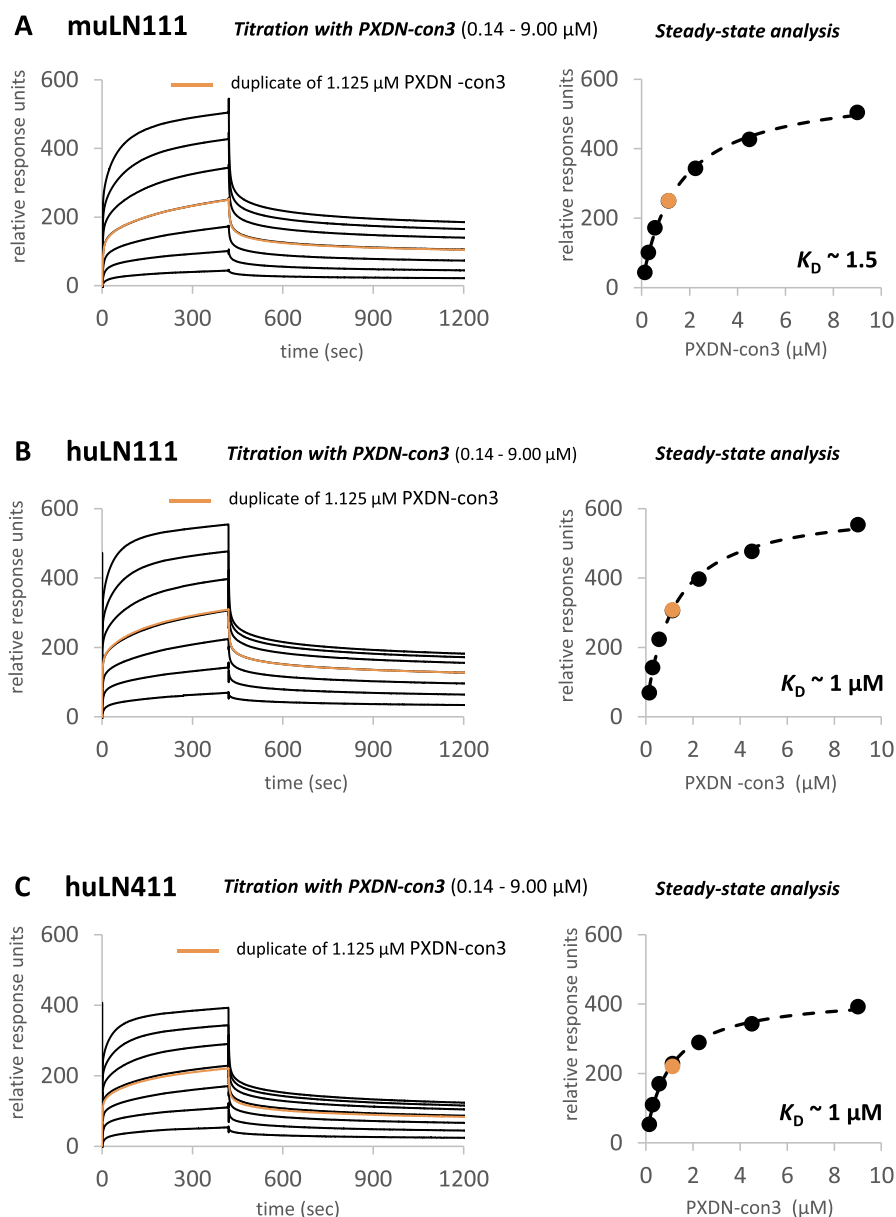


**Fig. 3. Kinetics and affinity of binding of human peroxidasin-1 construct, PXDN-con3, to murine and human laminins.** Determination of the dissociation constants ( $K_D$ ) for the interaction of different laminin isoforms with PXDN-con3 via steady-state analysis of double-referenced multi-cycle kinetics SPR experiments. Left: Titrations of (A) murine laminin-111 (muLN111), (B) human laminin-111 (huLN111) and (C) human laminin-411 (huLN411) with 7 different concentrations of PXDN-con3 (0.14–9.00  $\mu\text{M}$ ). Right: Corresponding plots of analyte concentrations versus steady-state responses and the affinities ( $K_D$ ) determined thereof. All plots are representatives of 3 independent measurements.



precipitation of BME proteins. By contrast, trimeric construct 2 and monomeric construct 4 (Fig. 2A) and monomeric construct 5 (not shown) did not interact with BME under the applied conditions indicating that the LRR domain plays an important role in binding of BME proteins.

Next, we screened the IP mixtures with antibodies raised against laminin resulting in the discovery of laminin as an interacting partner of peroxidasin construct PXDN-con3 (Fig. 2B). Typically, under reducing conditions, the three glycosylated chains of laminin appear as two bands on the gel, one at ~300 kDa corresponding to the  $\beta$ -chain and  $\gamma$ -chain (theoretical protein molar masses of 230 kDa and 220 kDa, respectively) and ~500 kDa indicative of the  $\alpha$ -chain (theoretical protein molar mass ~400 kDa) [24,25]. The band at around 200 kDa may represent a proteolytic fragment of laminin, which is still recognized by the anti-laminin antibody. It should also be noted that the IP mixture containing PXDN-con4 also showed a faint band at ~500 kDa upon staining with the anti-laminin antibody, suggesting a weak interaction of this construct with laminin.

### 3.2. The leucine-rich repeat domain of human peroxidasin 1 promotes binding to laminin

The interaction of PXDN-con3 with murine and human laminin-111 was confirmed and characterised by SPR spectroscopy, with laminin-111 serving as the ligand covalently coupled to the chip. Multi-cycle kinetics (MCK) experiments were performed using increasing concentrations of PXDN-con3. Fig. 3A (left) shows the sensorgram of PXDN-con3 associating with, and dissociating from, murine laminin-111 (muLN111), the best characterised laminin isoform [24,25]. Both the association and the dissociation occur in a multi-phasic manner, most probably as a consequence of the heterogeneous orientation of the amine coupled ligand on the chip surface, and the resulting variations in accessibility of the binding site(s). The double-referenced MCK experiments were analysed by plotting the response values 4 s before the injection stop (i.e. under steady-state conditions) against the respective PXDN-con3 concentration. The entire data set was then fitted to a steady-state affinity model resulting in a dissociation constant ( $K_D$ ) of 1.5  $\mu$ M, confirming that PXDN-con3 interacts specifically with laminin, and quantifying this binding (Fig. 3A, right).

To probe whether laminin binding to PXDN-con3 is species or isoform-dependent, human laminin-111 (huLN111) and human laminin-411 (huLN411) were covalently coupled to the chip surface and titrated

with PXDN-con3 as described above for muLN111. Similar binding curves to those obtained for muLN111, were obtained for huLN111 and huLN411 (Fig. 3B and C, left). Steady-state evaluation of the concentration dependent and saturable response curves (Fig. 3B and C, right) resulted in very similar  $K_D$  values, clearly indicating that the modes of binding of PXDN-con3 to muLN111 and huLN111, as well as isoform huLN411, are almost identical.

Since the immunoblots of the IP mixture containing PXDN-con4 also indicated some weak interaction with laminin, SPR measurements were also performed with PXDN-con4 and PXDN-con5 with muLN111. Fig. 4A depicts the sensorgram of the interaction of PXDN-con4 with muLN111. The shapes of the response curves are similar to PXDN-con3, but the maximum experimental response (~61 RU) was only ~14% of the maximum theoretical calculated response (~446 RU). Nevertheless, steady-state analysis resulted in a similar dissociation constant (2.0  $\mu$ M) as for PXDN-con3 (Fig. 4B). The titration with PXDN-con5 (Fig. 4C and D) gave 60% of the maximum theoretical response, but the  $K_D$  value was ~10 fold higher (i.e.: ~15  $\mu$ M) compared to the PXDN-con3 and PXDN-con4 constructs.

## 4. Discussion

Human peroxidasin 1 is an indispensable player in the basement membrane synthesis [15,16,22]. Loss of integrity of the BM is associated with severe developmental defects and pathologies [2,3]. Assembly of collagen IV generates one of the two major protein networks of BMs. It assembles through oligomerization and non-covalent interactions, and is subsequently stabilized by covalent cross-links including the sulfilimine bonds synthesized by PXDN, and the allysine-derived cross-links generated by lysyl oxidase and lysyl oxidase-like enzymes [26]. However, it unknown how the highly reactive and potentially damaging hypobromous acid [27] released by PXDN is able to generate specific S=N bonds between adjacent collagen IV protomers, without damaging neighbouring sites on collagen IV, or other BM molecules.

Together with thyroid peroxidase (TPO), PXDN catalyses an anabolic reaction. In contrast to (diffusible) lactoperoxidase (LPO), eosinophil peroxidase (EPO) and MPO, that each consist solely of a peroxidase domain, and are involved in non-specific immune defense reactions, TPO is a membrane-anchored peroxidase, and PXDN contains several non-enzymatic domains that might be expected to integrate and regulate the peroxidase activity of peroxidasin 1. Although differing in their structural composition, the main enzymatic reaction of all five

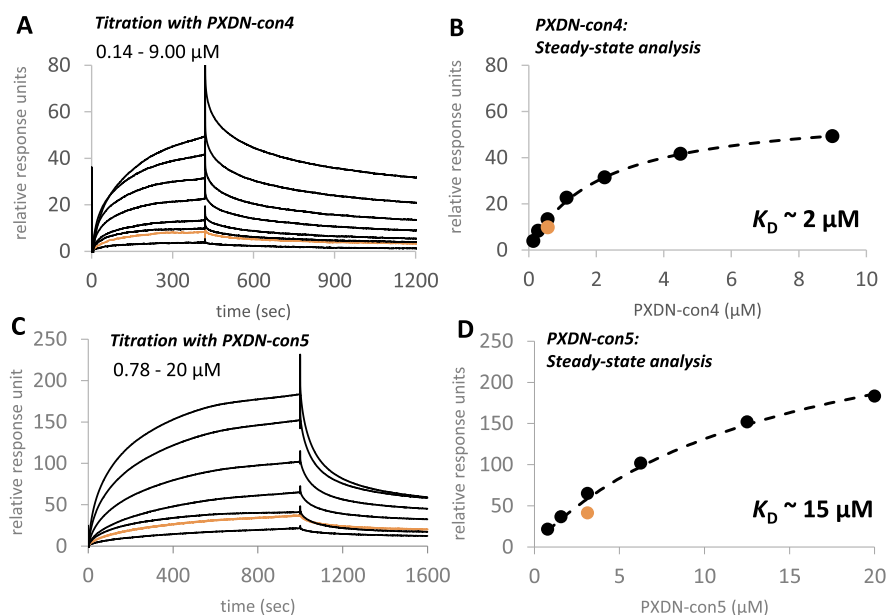


**Fig. 4.** Interaction between murine laminin-111 with human peroxidasin-1 constructs PXDN-con4 and PXDN-con5. Titration of murine laminin-111 (muLN111) with 0.14–9.00  $\mu$ M PXDN-con4 and 0.78–20  $\mu$ M PXDN-con5, respectively. Double-referenced multi-cycle kinetics SPR experiments with PXDN-con4 (A) and PXDN-con5 (C). Corresponding plots of the equilibrium response units versus PXDN-con4 (B) and PXDN-con5 (D) concentrations and the determined  $K_D$  values. The orange curves represent duplicates of 0.5625  $\mu$ M of PXDN-con4, and 3.15  $\mu$ M of PXDN-con5, respectively. (For interpretation of the references to colour in this figure legend, the reader is referred to the Web version of this article.)

human heme peroxidases is two-electron oxidation of halide and pseudohalide (thiocyanate) anions to the corresponding hypohalous acids and hypothiocyanite, which are diffusible antimicrobial oxidants. The capacity of those peroxidases to oxidize different anions depends strongly on the post-translational modifications of the heme and consequent alterations to the redox properties of the heme iron [21,28–32]. Human peroxidase 1 is able to efficiently oxidize bromide to hypobromous acid (HOBr), but not chloride to hypochlorous acid (HOCl) [21]. To date it is unknown as whether, and how, the PXDN-typical domains might restrict its mobility within the ECM, and foster the colocalisation of the peroxidase domain with the NC1 domains of collagen IV to avoid unspecific reactions of HOBr. So far, potential interaction partners of the ECM networks and associated proteins could not be identified.

In the present study, we have produced four different recombinant constructs of PXDN with distinct domain compositions (Fig. 1). One of the constructs, PXDN-con2 is trimeric, since it contains the alpha-helical linker region and redox-sensitive cysteines close to the C-terminus of the peroxidase domain, which are responsible for trimerization [23]. In contrast, PXDN-con3, PXDN-con4 and PXDN-con5 are monomeric proteins [23]. Upon association of these four His-tagged proteins with the anti-His<sub>6</sub> antibody coupled Dynabeads and mixing with BME, only laminin was immunoprecipitated, as demonstrated by SDS-PAGE and immunoblotting using polyclonal antibodies raised against laminin (Fig. 2). This supports and confirms the conclusion that type IV collagen does not form a stable complex with peroxidase 1, as reported recently [33]. These data suggest that interaction of PXDN with collagen IV and its NC1 domains, may be transient in nature or mediated by another ECM protein, such as the laminin isoforms described here.

The LRR domain in PXDN-con3 (Fig. 2B, lane 2) appears to be essential for efficient immunoprecipitation of laminin. Neither trimeric PXDN-con2, nor monomeric PXDN-con4 were able to promote precipitation of ECM proteins. The affinity of PXDN-con3 towards human and mouse laminin-111 (i.e.  $\alpha 1\beta 1\gamma 1$ ) was almost identical, suggesting the presence of conserved binding motif(s). Moreover, laminin-411 ( $\alpha 4\beta 1\gamma 1$ ), which contains a shorter  $\alpha$ -chain due to an N-terminal truncation, also bound to PXDN-con3 with a similar affinity. This suggests that the N-terminal region of the  $\alpha$ -chain of laminin is not essential for binding of PXDN.

To date, there is an absence of high resolution structural data of full length homotrimeric PXDN, or truncated variants. A potential reason for this lack of structural data is the high flexibility of both the monomeric and homotrimeric structures as demonstrated recently by small-angle X-ray scattering (SAXS) [23]. This SAXS data indicates that the POX domain (i.e. PXDN-con5) has an N-terminal flexible propeptide region and a compact globular core catalytic structure, similar to that of proMPO [34]. The monomeric construct PXDN-con4, which includes the four Ig domains located N-terminally of the propeptide region of the POX domain, is highly catalytically active [21,35]. The Ig domains have been shown to support correct folding of the POX domain [18,21] and thus to be essential for efficient sulfilimine bond formation in collagen IV [33]. Both SAXS data and rotary shadowing images suggest significant interaction of the Ig domains with the peroxidase domain and with each other [34]. The homotrimeric construct PXDN-con2 differs from PXDN-con4 at the C-terminus, with PXDN-con2 containing the additional VWC domain. The latter is not involved in trimerization, and is removed before secretion of peroxidase 1 to the ECM [36]. It should be noted that in the expression system used here, this processing step does not, or only partially, occurs [34]. In any case, trimerization is promoted by the amphipathic helix as well as by the conserved cysteines C736 and C1315. SAXS data as well as rotary shadowing, suggest a triangular arrangement of the three compact core peroxidase domains [34]. Moreover, modelling suggests free access for substrates (hydrogen peroxide and bromide) to the respective heme cavities in this trimeric construct [34]. A triangular arrangement of the POX domains is also obvious by inspection of micrograph data of full length trimeric

peroxidase from *Drosophila* [37]. The structures show a relatively compact core similar to the triangular POX domains as seen in the SAXS data [23,34]. The POX domains extend into three flexible arms, which are most likely composed of the LRR and Ig domains [37].

Unfortunately, an in-solution structure of PXDN-con3 is not available so far, nor is anything known about the molecular basis of the affinity of this construct to huLN111, muLN111 or huLN411. However, our SPR data indicate that the POX domain must be involved in binding to laminin. The measured SPR responses and calculated  $K_D$  values of PXDN-con4 and PXDN-con5 can be discussed on the basis of the available structural data of peroxidase variants outlined above. In general, the binding capacity of the SPR chip surface depends on the levels of immobilized laminin. The term maximum response ( $R_{max}$ ) describes the binding capacity of the surface in terms of the response at saturation. A theoretical  $R_{max}$  value can be calculated assuming 1:1 binding and both the immobilized ligand and the analyte (i.e. PXDN constructs) are active and fully accessible:

$$\text{Theoretical } R_{max} = \frac{\text{analyte MW}}{\text{ligand MW}} \times \text{RU}_{\text{immobilized ligand}}$$

The theoretical  $R_{max}$  for binding of PXDN-con3 to muLN111 is ~532 RU, whereas the experimental value was measured as ~524 RU, which is about 99% of the theoretical value. This is consistent with fully active ligand and analyte. Compared to the theoretical  $R_{max}$  of 446 RU of PXDN-con4 binding to muLN111, the experimental  $R_{max}$  is 61 RU, which is only 14% of the theoretical  $R_{max}$ . The POX domain in PXDN-con4 is well folded but highly shielded by the very flexible Ig domains as seen in the SAXS data [23]. As a consequence, there is a steric hindrance for the interaction between muLN111 and the POX domain in PXDN-con4. Keeping in mind the high flexibility of the protein, it can be assumed that at a distinct time point, only in a certain fraction of PXDN-con4 molecules, the arrangement of Ig and POX domains allows binding to laminin. In contrast, in the absence of the Ig domains (i.e. PXDN-con5), the accessibility to the POX domain for laminin is higher (reflected by 60% of the measured response), but the affinity is significantly lower due to partial misfolding of the catalytic domain in the absence of the stabilizing Ig domains. This might also apply to trimeric PXDN-con2, which lacks both Ig and LRR domains and was not able to immunoprecipitate laminin (Fig. 2). As mentioned above, we could not study the interaction between laminin and full length homotrimeric PXDN, which may alter the thermodynamics of binding. Based on the available data, we hypothesize that the presence of the LRR domain in PXDN-con3 impairs intimate interaction between the Ig domains, thereby providing accessibility to the correctly folded catalytic domain, which is supported by the micrograph of full length peroxidase from *Drosophila* described above and in Ref. [37]. Thus, the LRR domain appears to promote high affinity binding of laminin-111 to the POX domain of human peroxidase 1.

Whilst these data provide compelling information on the binding of human peroxidase 1 to laminins, a number of critical questions remain. These include the binding site(s) and chains from the laminin that are involved, and the mode of interaction of the laminin-peroxidase complex with type IV collagen, and specifically the NC1 domains. Furthermore, the source of hydrogen peroxide, which is essential for the catalytic activity of PXDN and bromide oxidation is unclear, with recent studies appearing to eliminate NADPH oxidases as a source [38,39]. Structural studies on potential complexes in-solution and/or by electron microscopy would clearly be beneficial.

## Acknowledgements

This work was supported by the Austrian Science Fund, FWF [Doctoral Program BioToP-Molecular Technology of Proteins (W1224) and project P25538]. Additional financial support from the Novo Nordisk Foundation and Danmarks Frie Forskningsfond (grants NNF13OC0004294 and DFF-7014-00047, respectively, to MJD) is

gratefully acknowledged. The SPR equipment was kindly provided by the EQ-BOKU VIBT GmbH and the BOKU Core Facility Biomolecular & Cellular Analysis.

## References

- [1] S. Colon, P. Page-McCaw, G. Bhave, *Antioxidants Redox Signal.* 27 (2017) 839–854.
- [2] A. Pozzi, P.D. Yurchenco, R.V. Iozzo, *Matrix Biol.* 57–58 (2017) 1–11.
- [3] R. Jayadev, D.R. Sherwood, *Curr. Biol.* 27 (2017) R207–R211.
- [4] E. Hohenester, P.D. Yurchenco, *Cell Adhes. Migrat.* 7 (2013) 56–63.
- [5] M. Durbeej, *Cell Tissue Res.* 339 (2010) 259–268.
- [6] M. Aumailley, L. Bruckner-Tuderman, W.G. Carter, R. Deutzmann, D. Edgar, P. Ekblom, J. Engel, E. Engvall, E. Hohenester, J.C. Jones, H.K. Kleinman, M.P. Marinkovich, G.R. Martin, U. Mayer, G. Meneguzzi, J.H. Miner, K. Miyazaki, M. Patarroyo, M. Paulsson, V. Quaranta, J.R. Sanes, Z. Sasaki, K. Sekiguchi, L.M. Sorokin, J.F. Talts, K. Tryggvason, J. Uitto, I. Virtanen, K. von der Mark, U.M. Wewer, Y. Yamada, P.D. Yurchenco, *Matrix Biol.* 24 (2005) 326–332.
- [7] J.H. Miner, *Microsc. Res. Tech.* 71 (2008) 349–356.
- [8] C.Y. Chuang, G. Degendorfer, M.J. Davies, *Free Radic. Res.* 48 (2014) 970–989.
- [9] G. Degendorfer, C.Y. Chuang, A. Hammer, E. Malle, M.J. Davies, *Free Radic. Biol. Med.* 89 (2015) 721–733.
- [10] G. Degendorfer, C.Y. Chuang, M. Mariotti, A. Hammer, G. Hoefler, P. Hagglund, E. Malle, S.G. Wise, M.J. Davies, *Free Radic. Biol. Med.* 115 (2018) 219–231.
- [11] T. Nybo, S. Dieterich, L.F. Gamon, C.Y. Chuang, A. Hammer, G. Hoefler, E. Malle, A. Rogowska-Wrzesinska, M.J. Davies, *Redox Biol.* 20 (2019) 496–513.
- [12] S. Baldus, J.P. Eiserich, A. Mani, L. Castro, M. Figueroa, P. Chumley, W. Ma, A. Tousson, C.R. White, D.C. Bullard, M.L. Brennan, A.J. Lusic, K.P. Moore, B.A. Freeman, *J. Clin. Invest.* 108 (2001) 1759–1770.
- [13] H. Cai, C.Y. Chuang, C.L. Hawkins, M.J. Davies, *Sci. Rep.* 10 (2020) 666.
- [14] M.D. Rees, J.M. Whitelock, E. Malle, C.Y. Chuang, R.V. Iozzo, A. Nilasaroya, M.J. Davies, *Matrix Biol.* 29 (2012) 63–73.
- [15] G. Bhave, C.F. Cummings, R.M. Vanacore, C. Kumagai-Cresse, I.A. Ero-Tolliver, M. Rafi, J.S. Kang, V. Pedchenko, L.I. Fessler, J.H. Fessler, B.G. Hudson, *Nat. Chem. Biol.* 8 (2012) 784–790.
- [16] A.S. McCall, C.F. Cummings, G. Bhave, R. Vanacore, A. Page-McCaw, B.G. Hudson, *Cell* 157 (2014) 1380–1392.
- [17] M. Soudi, M. Zamocky, C. Jakopitsch, P.G. Furtmüller, C. Obinger, *Chem. Biodivers.* 9 (2012) 1776–1793.
- [18] M. Soudi, M. Paumann-Page, C. Delporte, K.F. Pirker, M. Bellei, E. Edenhofer, G. Stadlmayr, G. Battistuzzi, K.Z. Boudjeltia, P.G. Furtmüller, P. Van Antwerpen, C. Obinger, *J. Biol. Chem.* 290 (2015) 10876–10890.
- [19] M. Zamocky, S. Hofbauer, I. Schaffner, B. Gasselhuber, A. Nicolussi, M. Soudi, K.F. Pirker, P.G. Furtmüller, C. Obinger, *Arch. Biochem. Biophys.* 574 (2015) 108–119.
- [20] M. Zamocky, C. Jakopitsch, P.G. Furtmüller, C. Dunand, C. Obinger, *Proteins* 72 (2008) 589–605.
- [21] M. Paumann-Page, R.S. Katz, M. Bellei, I. Schwartz, E. Edenhofer, B. Sevcnikar, M. Soudi, S. Hofbauer, G. Battistuzzi, P.G. Furtmüller, C. Obinger, *J. Biol. Chem.* 292 (2017) 4583–4592.
- [22] E. Lazar, Z. Peterfi, G. Sirokmany, H.A. Kovacs, E. Klement, K.F. Medzihradsky, M. Geiszt, *Free Radic. Biol. Med.* 83 (2015) 273–282.
- [23] M. Paumann-Page, R. Tscheliessnig, B. Sevcnikar, R.S. Katz, I. Schwartz, S. Hofbauer, V. Pfanzagl, P.G. Furtmüller, C. Obinger, *Biochim. Biophys. Acta* (2019) 140249.
- [24] R. Timpl, H. Rohde, P.G. Robey, S.I. Rennard, J.M. Foidart, G.R. Martin, *J. Biol. Chem.* 254 (1979) 9933–9937.
- [25] T. Sasaki, R. Fassler, E. Hohenester, *J. Cell Biol.* 164 (2004) 959–963.
- [26] C. Añazco, A.J. López-Jiménez, M. Rafi, L. Vega-Montoto, M.-Z. Zhang, B.G. Hudson, R.M. Vanacore, *J. Biol. Chem.* 291 (2016) 25999–26012.
- [27] D.I. Pattison, M.J. Davies, *Biochemistry* 43 (2004) 4799–4809.
- [28] J. Arnhold, P.G. Furtmüller, C. Obinger, *Redox Rep.* 8 (2003) 179–186.
- [29] P.G. Furtmüller, J. Arnhold, W. Jantschko, C. Jakopitsch, C. Obinger, *J. Inorg. Biochem.* 99 (2005) 1220–1229.
- [30] J. Arnhold, E. Monzani, P.G. Furtmüller, L. Casella, M. Zederbauer, C. Obinger, *Eur. J. Inorg. Chem.* 19 (2006) 3801–3811.
- [31] G. Battistuzzi, M. Bellei, P.G. Furtmüller, M. Zederbauer, M. Sola, C. Obinger, *Biochemistry* 45 (2006) 12750–12755.
- [32] G. Battistuzzi, J. Stampfer, M. Bellei, J. Vlasits, M. Soudi, P.G. Furtmüller, C. Obinger, *Biochemistry* 50 (2011) 7987–7994.
- [33] L.A. Ero-Tolliver, B.G. Hudson, G. Bhave, *J. Biol. Chem.* 290 (2015) 21741–21748.
- [34] I. Grishkovskaya, M. Paumann-Page, R. Tscheliessnig, J. Stampfer, S. Hofbauer, M. Soudi, B. Sevcnikar, C. Oostenbrink, P.G. Furtmüller, K. Djinović-Carugo, W.M. Nauseef, C. Obinger, *J. Biol. Chem.* 292 (2017) 8244–8261.
- [35] B. Sevcnikar, M. Paumann-Page, S. Hofbauer, V. Pfanzagl, P.G. Furtmüller, C. Obinger, *Arch. Biochem. Biophys.* 681 (2020) 108267.
- [36] S. Colon, G. Bhave, *J. Biol. Chem.* 291 (2016) 24009–24016.
- [37] R.E. Nelson, L.I. Fessler, Y. Takagi, B. Blumberg, D.R. Keene, P.F. Olson, C.G. Parker, J.H. Fessler, *EMBO J.* 13 (1994) 3438–3447.
- [38] G. Sirokmany, H.A. Kovács, E. Lázár, K. Kónya, A. Donkó, B. Enyedi, H. Grasberger, M. Geiszt, *Redox Biol.* 16 (2018) 314–321.
- [39] G. Sirokmany, M. Geiszt, *Front. Immunol.* 10 (2019) 394.